

Effect of Fe_2O_3 additives on the sintering mechanism of a high strength ceramsite from a CFB fly ash

Ikechukwu Okeke, Peng Liyang, Yuhong Qin*, Chukwubuike Chiamera Onwuagbu, Afreh Paul, Maywish Islam

College of Environment and Ecology, Taiyuan University of Technology, Taiyuan, Shanxi Province, China.

*Corresponding Author

Received: 27 May 2025,

Received in revised form: 25 Jun 2025,

Accepted: 28 Jun 2025,

Available online: 03 Jul 2025

©2025 The Author(s). Published by AI
Publication. This is an open-access article
under the CC BY license

Keywords— CFB fly ash, Fe_2O_3 , ceramsite,
sintering mechanism, liquid-phase
sintering, compressive strength

Abstract— The sustainable reutilization of industrial solid waste offers a viable strategy to address environmental concerns associated with coal-fired power generation. This study investigates the role of Fe_2O_3 additives in enhancing the sintering behavior, microstructural evolution, and structural properties of high-strength ceramsite synthesized from circulating fluidized bed (CFB) fly ash. A series of ceramsite samples with varying Fe_2O_3 contents (0–15 wt%) were sintered at temperatures ranging from 1150°C to 1300°C to evaluate the influence of Fe_2O_3 on material performance. The results revealed that the addition of 5 – 10 wt% Fe_2O_3 at 1300°C produced optimal results. Microstructural analyses using X-ray diffraction (XRD), scanning electron microscopy (SEM), and thermogravimetric–differential scanning calorimetry coupled with Fourier-transform infrared spectroscopy (TG-DSC-FTIR) demonstrated that Fe_2O_3 effectively promotes liquid-phase sintering, facilitates mullite crystallization, and improves particle bonding and densification, while simultaneously moderating gas evolution. However, excessive Fe_2O_3 content (>10 wt%) led to reduced strength and densification due to increased porosity and decreased liquid-phase viscosity. This research not only highlights the dual function of Fe_2O_3 as both a fluxing and structural stabilizing agent but also provides a practical route for converting coal-based solid waste into high-performance construction materials. The findings contribute to the advancement of sustainable building technologies and support circular economy goals through efficient resource recovery and waste minimization.

I. INTRODUCTION

When coal is burned in a circulating fluidized bed combustion (CFBC) boiler, it produces circulating fluidized bed (CFB) fly ash that is significantly different from traditional pulverized fuel combustion fly ash. This is as a result of different combustion conditions which produce fly ash with different mineralogic composition, chemical properties, and structure, which ultimately not only makes CFB fly ash less desirable to use, it also makes it more difficult to use compared to pulverized fly ash [1], [2]. With

China producing approximately 80–150 million tonnes of CFB fly ash every year, there is a growing need to consider more effective ways to reuse as much CFB fly ash as possible [3]. The physical properties of CFB fly ash do not help its case for use. Unlike pulverized fly ash, many of the CFB fly ash have a distinctly irregular shapes, either blocky or rod-like, along with a very rough, porous, and loosely-bound surface. These characteristics are simply caused by the lack of sufficient liquid phase at combustion temperatures (850–900°C) at which CFB ash is burning,

with resulting in lower densities and items having a rougher texture [4]. Additionally, during its cooling, the particles do not form the smooth and spherical glass structures typically formed in other fly ashes. The thermal decomposition of limestone and release of the CO_2 upon combustion contribute to the loose and porous nature of CFB fly ash [5], [6]. Qian et al. [7] propose that as anhydrite and clay minerals decrease in proportion, the particles are even more loosely structured. In order to address expansion problems, research has examined processing CFB fly ash into highly porous materials, and it has even been used as an expanding agent in self-leveling mortar [2]. CFB fly ash is also being adopted for various other industries such as binder production, construction materials, road infrastructure, and sulfate activation to contribute to sustainability development [8], [9], [10].

Ceramsite is a construction material that possesses good mechanical resistance in both acidic and alkaline environments, high strength, and high-performing thermal insulation properties [11]. Based on composition (Fe_2O_3 , Al_2O_3 , SiO_2), ceramsite also shows potential as an effective medium for filtration in industrial wastewater and municipal wastewater treatment systems. Ceramsite is a major component of the construction industry as it is used in making bricks, aggregates for concrete and ceramic-based products [12]. Due to both stability and if being lightweight with high insulation properties, ceramsite has useful applications in a broad spectrum of industries including agriculture, metallurgy, construction and chemical manufacturing [13]. Amid the growing demand for sustainable waste management, research efforts are focused on investigating solid waste-derived materials in the production of high-strength ceramsite. Potential raw materials that have been explored include fly ash, incineration fly ash [14], [15], river sediments [16], industrial tailings [17], sludge [18], [19] coal gangue, red mud, and electrolytic manganese slag [20]. The interest in solid waste recycling is increasingly important to this research avenue [21]. High-strength ceramsite is an artificial lightweight aggregate that is known for its load-bearing capacity, with a cylindrical compressive strength greater than 4.0 MPa and stacking density of 500 to 1200 kg/m^3 . It is made through a multi-step process which entails: raw material preparation, granulation, and sintering at high temperatures [22], [23]. In the latter, CFB fly ash serves several important purposes, such as to provide SiO_2 and Al_2O_3 , which make up the structure, to add CaO , MgO , and Fe_2O_3 , which are fluxing agents to aid sintering, and to add C and CaCO_3 , which act as gas-forming agents to produce porosity and lightweight aggregate [24].

Sintering is an important process to treat fly ash. Fly ash is mixed with silica-alumina materials and fluxing

agents to partial melting of the material in the kiln at fixed high temperatures, then, is cooled to solidify. This high-temperature treatment is necessary to detoxify organic contaminants such as dioxins while binding heavy metals, which increases environmental safety of materials made from fly ash [15], [25]. The sintering procedure applied to fly ash shares many similarities with the method used in ceramsite production [26]. The high-temperature treatment of sintering limits the leaching of ion exchange with ceramsite and provides chemical stability to the ceramsite which makes it suitable in encapsulating heavy metals [27]. Therefore, ceramsite made from fly ash by sintering will always show great stability and durability while eliminating leaching and maintaining environmental safety, making them suitable in all construction applications.

However, sintering inevitably generates emissions of harmful gases such as SO_2 , NO_x , and CO . Research by Liu et al. [27] indicates that SO_2 is the most significant sulfur-based pollutant released in this process, with approximately 50% originating from the reduction of calcium and magnesium sulfates and another 40% from the combustion of organic sulfur compounds and sulfite decomposition. The degree to which these emissions occur depends on factors such as the sintering atmosphere, airflow, and water vapor levels. Yu et al. [14] examined the influence of sintering temperature and additives on Al_2O_3 ceramics, identifying that refining the sintering conditions increases the relative density and the mechanical strength. The basic oxides, Fe_2O_3 , CaO , or MgO , included or added, amplify the accumulation of crystals and liquid phase that are needed to increase the property of the sintered ceramsite. Similarly, Ma et al. [28] studied the production of ceramic foams by adding 8 wt% of MgO when investigating Al_2O_3 ceramics with varied levels of flux and sintering temperature which ultimately lead to increased compressive strength.

The production of alumina creates red mud, which is a significant waste by-product. Red mud has a high concentration of Fe_2O_3 . According to Wang et al. [29], Fe_2O_3 was the most abundant mineral compound in red mud, which comprised of 59.37% of the red mud components. Due to the high concentration of iron, black cores develop, and inter-particle adhesion is limited during ceramsite formation, which can have a great deal of impact on the structure overall [30]. Pei et al. [31] examined the incorporation of red mud in combination with various materials to produce ultra-lightweight ceramsite, finding that Fe_2O_3 accounted for approximately 53.96% of the red mud mass. Their results also indicated that as red mud content increased, the bulk density of ceramsite decreased initially but increased thereafter, indicating a complex interaction between additive content and density.

Mi et al. [32] conducted a similar study in which they used both fly ash and red mud as raw materials to produce high strength ceramsite. In the study, the authors examined the ratios of raw materials and sintering conditions. It is reported that the best composition produced a ceramsite with a compressive strength of 21.01 MPa. Mi et al. [32] reported an increase in Fe_2O_3 resulted in a ceramsite with a higher density and burned at a lower sintering temperature. The best outcome was Fe_2O_3 content of approximately 6-8% as the overall trends observed were porosity, and general strength of the ceramsite improved with increasing sintering temperature. Zou et al. [33] confirmed this observation, stating that to achieve optimum mechanical performance of sintered ceramsite, raw material Fe_2O_3 concentrations were held at about 5% to 8%. Taken together, the studies have established the functional significance of Fe_2O_3 in CFB fly ash. In addition, the amount of Fe_2O_3 content was determined to only affect the initial conditions of the sintering process for producing high-strength ceramsite.

This study aimed to investigate the effect of sintering temperature and Fe_2O_3 concentration on the formation and properties of ceramsite. With CFB fly ash serving as the primary raw material, Fe_2O_3 was introduced as a flux to improve the sintering process. The research evaluated fundamental physical attributes, including compressive strength, apparent density, stacking density, and water absorption. To obtain a detailed perspective on the sintering process, advanced in situ high-temperature observation methods were employed alongside XRD, TG-DSC-FTIR, and SEM analyses. A key focus was understanding how Fe_2O_3 contributes to phase transitions, microstructural

evolution, and the final performance of high-strength CFB fly ash ceramsite.

II. MATERIALS AND METHOD

2.1 Raw materials

This research utilized Fe_2O_3 and CFB fly ash as raw materials, with the CFB fly ash sourced from Shanxi Pingshuo Gangue Power Generation Co., Ltd., a major coal-based solid waste processing and power generation enterprise in Shanxi Province, China. The Fe_2O_3 additive, obtained from Taiyuan Biochemical Technology Co., Ltd., had a purity of over 98%, ensuring its suitability for precise experimental analysis. To determine the chemical composition of the CFB fly ash, X-ray fluorescence spectrometry (XRF) was performed in accordance with the GB/T 176–2017 standard, requiring the sample to be heated to 950°C for 60 min [22]. Loss on ignition (LOI) was also analyzed, with results summarized in Table 1. The XRF analysis showed that SiO_2 and Al_2O_3 were the dominant oxides, comprising 87.77% of the material, while Fe_2O_3 , CaO , MgO , Na_2O , and K_2O accounted for 7.25%. These values confirm that CFB fly ash meets the chemical criteria for ceramsite production [23]. To further examine its mineral structure, X-ray diffraction (XRD) analysis was conducted. As presented in Fig. 1, kyanite, quartz, and hematite were identified as the primary mineral phases, with anhydrite and lime appearing in smaller amounts. These findings offers an important insight into the mineral composition and structural properties of CFB fly ash.

Table 1. Chemical composition of the CFB fly ash

Component; wt.%													
Sample	SiO_2	Al_2O_3	CaO	Fe_2O_3	TiO_2	K_2O	Na_2O	MgO	SO_3	LOI	SiO_2	Al_2O_3	CaO
CFB fly ash	46.47	41.30	2.63	3.46	1.85	0.73	0.08	0.35	0.36	2.53	46.47	41.30	2.63

2.2 Preparation of ceramsite

This study systematically examined the impact of Fe_2O_3 on the physical and chemical properties of ceramsite by preparing 28 different sample sets using CFB fly ash and Fe_2O_3 under controlled conditions. The primary objective was to assess the role of Fe_2O_3 in enhancing ceramsite strength. The experimental design incorporated Fe_2O_3 at four different weight percentages (0 wt%, 5 wt%, 10 wt%, and 15 wt%), while sintering temperatures were set at seven levels: 1150°C, 1175°C, 1200°C, 1225°C, 1250°C, 1275°C, and 1300°C.

To ensure experimental consistency, the CFB fly ash was first dried at 105°C for 24 hours until it reached a stable weight. The dried material was then sieved through a 96 μm (160 mesh) square sieve to achieve uniformity in particle size. The required proportions of CFB fly ash and Fe_2O_3 were mixed using a cement mortar mixer, ensuring thorough homogenization before pelletization.

The formation of ceramic pellets (5–10 mm in diameter) was conducted using disc-pelletizing equipment, where the material mixture was combined with a small quantity of water and rotated at a speed of 20–50 r/min to achieve uniform granulation. Sintering was performed in a

KSL-1400X resistance furnace under a precisely controlled heating program. To prevent material cracking due to rapid temperature fluctuations, a 20-minute preheating step was introduced to facilitate gas release. The temperature was then gradually increased to 800°C at a rate of 5°C/min

before reaching the final sintering temperature, which was maintained for 60 minutes. Following sintering, the ceramsite samples were allowed to cool naturally inside the furnace until they reached 25°C before being collected for further evaluation

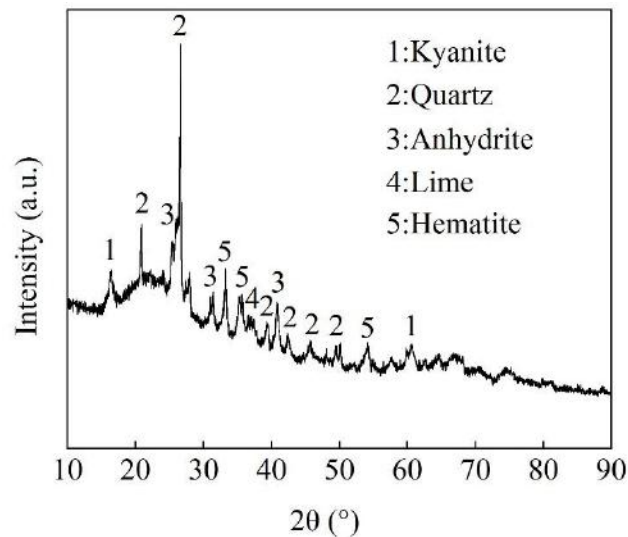


Fig. 1. XRD analysis of the CFB fly ash

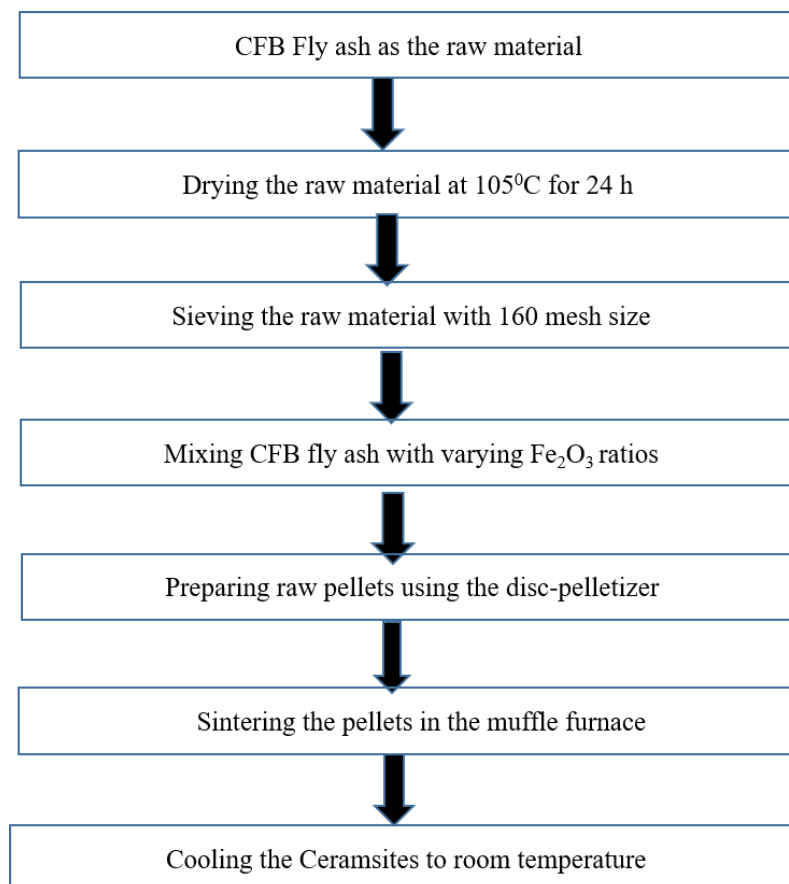


Fig 2. Flow chart showing the process of producing ceramsite

2.3 Evaluation of physical and chemical properties of ceramsite.

The mineral compositions of both CFB fly ash and sintered ceramsite were examined using X-ray diffraction (XRD). Prior to analysis, the ceramsite samples were crushed and finely ground until they could pass through a 45 μm square sieve.

To evaluate the physical properties of ceramsite, important parameters including apparent density, stacking density, one-hour water absorption, and cylindrical compressive strength were measured following the GB/T17431.2-2010 standard [34]. Due to the large number of ceramsite samples required for the cylindrical compressive strength test, manual pelletizing was not feasible. Instead, a computerized press (HYD-500KG, Dongguan Hongjin Testing Instrument Co., Ltd., China) was used to assess the failure load, which represents the maximum pressure at which the ceramsite sample breaks [34]. The compressive strength was then obtained by calculating the average failure load of twenty ceramsites using Eq. (1) [35], [36].

$$P = \frac{2.8P_c}{\pi X^2} \quad (1)$$

In this case, P stands for compression strength (MPa), X for ceramsite diameter (mm), and P_c for ceramsite rupture load (N).

The samples' apparent density, stacking density, and water absorption were measured using Eqs. (2), (3), and (4), respectively [34]. To improve the reliability of the data, each sample was tested twice, ensuring greater statistical accuracy.

$$\rho_{ap} = \frac{M1 \times 1000}{V1 - V0 - 500} \quad (2)$$

where ρ_{ap} stands for the apparent density measured in (kg/m^3), $m1$ stands for the mass of the dried sample measured in (g), $V1$ is the total volume of the sample, circular metal plate, or water and is measured in (mL), while $V0$ stands for the volume of the circular metal plate measured in (mL).

$$\rho_{bu} = \frac{(M2 - M3) \times 1000}{V2} \quad (3)$$

In this equation, ρ_{bu} stands for the stacking density measured in (kg/m^3), and then m_2 is the total mass of the sample and measuring cylinder measured in (g), while m_3 is the mass of the measuring cylinder (g), and V_2 is the volume of the measuring cylinder (ml).

The ratio of water absorption of the ceramsite after immersion in water for 1 h was calculated using Eq. (4):

$$\omega_a = \frac{m_0 - m_1}{m_1} \times 100\% \quad (4)$$

Where ω_a stands for 1-h water absorption of ceramsite calculated in %, m_0 is the mass of the sample after water absorption, while m_1 is the mass of the sample before absorption.

2.4 In situ analysis of the macroscopic morphology

Figure 3 illustrates the setup of the in situ high-temperature observation system, which includes a high-temperature furnace, a gas management system, and an image acquisition and processing unit. During the heating process, the morphology of the ceramsite was analyzed using ImageJ 1.46r software. The furnace used in the experiment was almost identical to the one utilized for ceramsite production.

To ensure a controlled environment, nitrogen gas (N_2) was introduced at a flow rate of 80 mL/min. This helped remove gases released during sintering while also cooling the quartz observation window. Image acquisition was conducted systematically: during the 30-minute constant temperature phase, images were captured every 10 minutes, and throughout the heating phase, images were taken at 10°C increments from 800°C to 1300°C . The estimated ceramsite area was analyzed using ImageJ 1.46r, and the shrinkage or expansion ratio was calculated based on Equation (5).

$$\frac{\text{Shrinkage}}{\text{Expansion}(\%)} = \frac{S_t - S_0}{S_0} \times 100\% \quad (5)$$

Where shrinkage or expansion is defined as the percentage change in the ceramsite's projected area, the ceramsite's projected area at a specific temperature, and the ceramsite's original projected area, mm^2 .

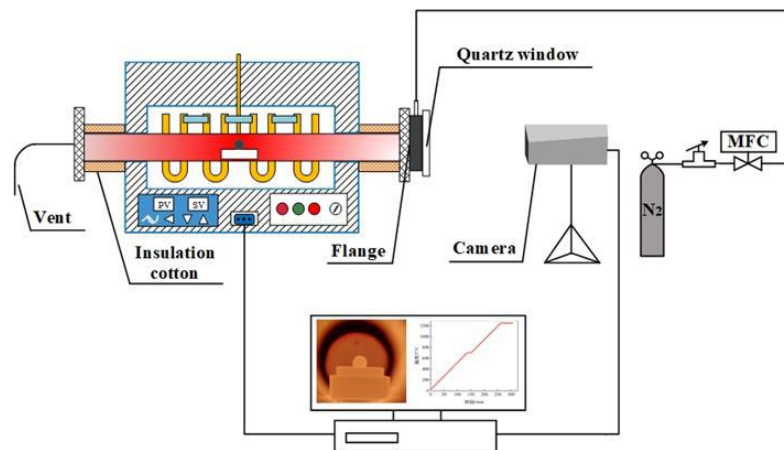


Fig. 3. An in situ observation instrument

III. RESULTS AND DISCUSSION

3.1. The effect of sintering temperature and Fe_2O_3 addition on ceramsite properties

The preparation of ceramsite is influenced by four key sintering parameters: sintering temperature, sintering time, preheating temperature [37], and preheating time [38]. Among these, sintering temperature is particularly important and must be carefully managed. If the temperature is too high, an excessive liquid phase forms,

which can weaken the ceramsite structure and cause particles to adhere to one another. Conversely, a temperature that is too low results in insufficient liquid phase formation, preventing proper densification.

The impact of Fe_2O_3 addition on ceramsite compressive strength at varying sintering temperatures is depicted in Fig. 4. As shown, the compressive strength of ceramsite increased with rising sintering temperatures.

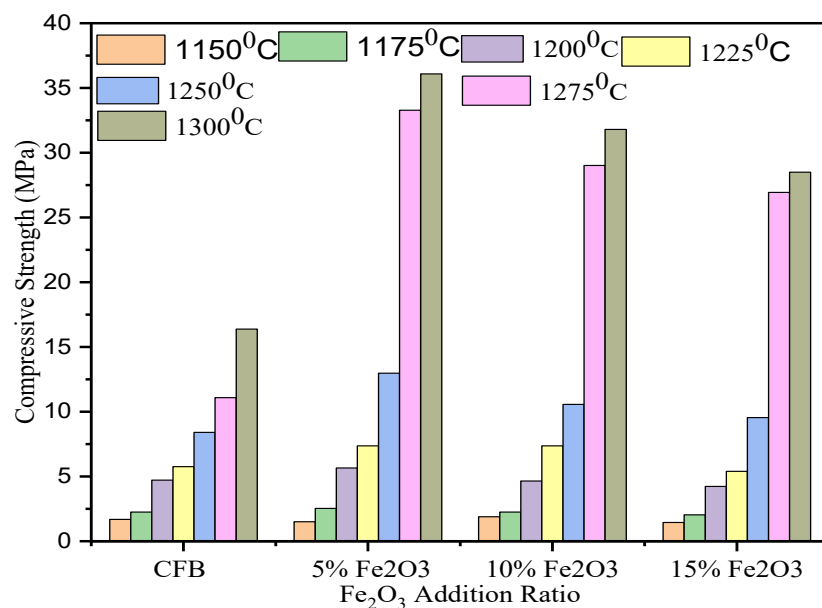


Fig. 4. Ceramsite's compressive strength with varying Fe_2O_3 additive ratios

The temperature at which ceramsite undergoes sintering has a significant impact on its compressive strength [32]. The data show that increasing the sintering temperature led to a steady rise in strength across all Fe_2O_3 additions. However, at 1150°C, the compressive strength remained low, ranging from 1.45 MPa to 1.89 MPa. This

was primarily due to insufficient sintering, as the particles had only just started to bond, resulting in weak structural cohesion. At 1175°C, the compressive strength improved noticeably, particularly with Fe_2O_3 additions from 5 wt% to 15 wt%. However, the strength still did not reach the 4 MPa requirement outlined in the Chinese National Standard

(GB/T 17431.1–2010) and the Chinese Engineering Construction Standard (T/CECS 10113–2020) [22], [23]. This was mainly due to the low silica-to-aluminum ($\text{SiO}_2/\text{Al}_2\text{O}_3$) ratio in CFB fly ash, which was below 1.5. Additionally, minerals such as mullite, anorthite, and corundum were difficult to melt at this temperature [39]. As a result, the ceramsite lacked sufficient liquid phase formation, which is necessary for effective particle bonding and the development of a strong crystalline structure.

The sintering temperature and Fe_2O_3 additives have a major impact on compressive strength. At all temperatures, the control sample containing 0 wt% Fe_2O_3 performed the worst. Its strength increased only moderately at higher temperatures, reaching 11.09 MPa at 1275°C and beyond, and was negligible at lower temperatures, ranging from 1.69 to 4.72 MPa at 1150–1200°C. Due to the lack of a fluxing agent, this suggests weak particle bonding and low densification. The 10 wt% Fe_2O_3 sample was significantly stronger compared to the sample without Fe_2O_3 additives, reaching 29.02 MPa at 1275°C and increasing to 31.80 MPa at 1300°C. Notably, the 15 wt% Fe_2O_3 sample reach a peak of 28.49 MPa at 1300°C. However, do not reach the strength of the 5 wt% Fe_2O_3 sample, demonstrating that strength is not always improved by increasing Fe_2O_3 ratios. The best performance was observed at 1300°C with a 5 wt% Fe_2O_3 addition, achieving a compressive strength of 36.09 MPa.

When Fe_2O_3 content exceeded 5 wt%, the reduction in liquid phase viscosity negatively affected internal gas discharge and pore formation [31]. However, the addition of Fe_2O_3 enhanced the fluxing properties of the raw material, facilitating liquid phase formation and supporting the development of the $\text{Fe}_2\text{O}_3\text{--Al}_2\text{O}_3\text{--SiO}_2$ oxide system within

the ceramsite. During sintering, the solid particles became more compact and recrystallized, which contributed to the overall increase in ceramsite's compressive strength [40]. The physical properties of ceramsite—such as water absorption, apparent density, and stacking density are closely tied to its strength and are influenced by factors like mineral composition and pore structure.

Figure 5 demonstrates how Fe_2O_3 content influences the physical properties of ceramsite at a sintering temperature of 1250°C. The sample containing 5 wt% Fe_2O_3 achieved the highest values for stacking density (944.55 kg/m^3) and apparent density (1890.68 kg/m^3), while maintaining a relatively low water absorption rate of 6.50%. Conversely, the sample with 15 wt% Fe_2O_3 at the same temperature exhibited slightly lower stacking and apparent densities of 936.67 kg/m^3 and 1764 kg/m^3 , respectively, and a higher water absorption rate of 8.08%. These findings suggest that the 5 wt% Fe_2O_3 addition significantly enhanced ceramsite densification, which is essential for improving its overall strength.

The significant enhancement in compressive strength can be attributed to the closure of pre-existing pores, which restricted moisture movement and improved the material's overall densification. However, the slight increase in water absorption in the 15 wt% Fe_2O_3 sample suggests that an excess of Fe_2O_3 may lead to non-uniform densification. This is likely due to overfluxing, which facilitates the formation of isolated pores, thereby reducing the effectiveness of the densification process. Ceramsites that are denser and have fewer pores are more effective and help harmful substances solidify [39], [40].

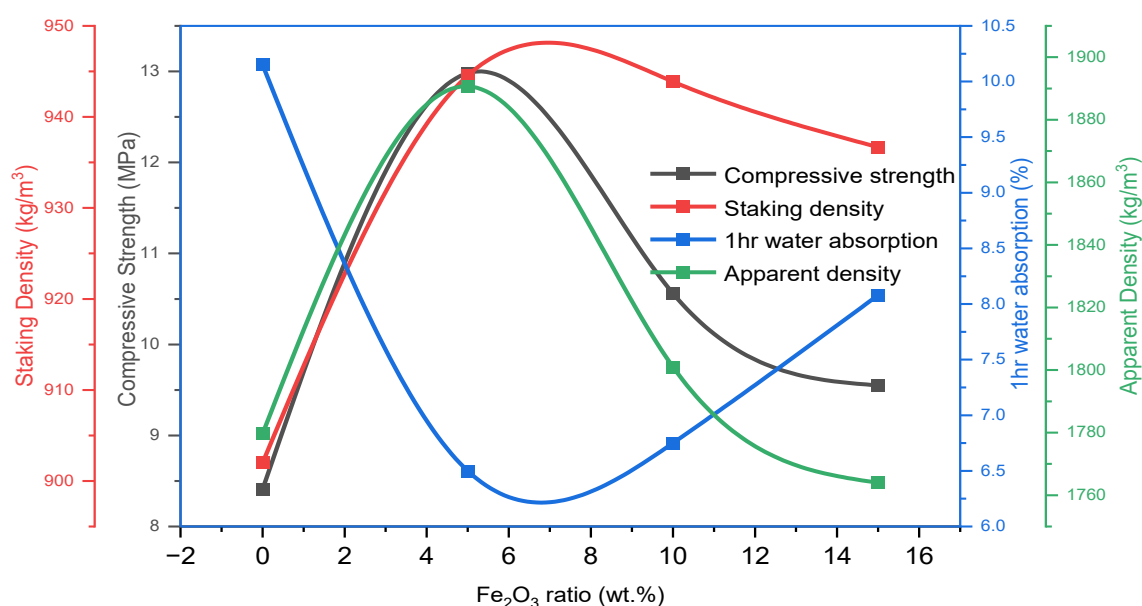


Fig. 5. Impact of Fe_2O_3 addition on ceramsite performance

At 5 wt% Fe_2O_3 addition and a sintering temperature of 1225°C , the ceramsite exhibited improved physical properties, with compressive strength rising to 7.36 MPa, water absorption measured at 12.20%, bulk density at 863.94 kg/m^3 , and apparent density at 1770.23 kg/m^3 . As the sintering temperature increased to 1300°C , the ceramsite's surface darkened, and a thick, enamel-like layer formed. Under these conditions, compressive strength peaked at 36.09 MPa, water absorption decreased significantly to 0.19%, bulk density rose to 1189.3 kg/m^3 , and apparent density reached 2327.85 kg/m^3 . These enhancements occurred due to a dynamic equilibrium between gas pressure, viscosity, and surface tension of the liquid phase, which facilitated a well-distributed pore structure and increased strength [41], [42].

3.2 Macroscopic morphology analysis

High-strength ceramsite is produced from CFB fly ash via high-temperature sintering. During this process, the raw

pellets experience expansion and contraction, reflecting the interplay of gas, liquid, and solid phases in ceramsite formation [41], [43]. By monitoring these changes and calculating the projected area variation using Equation (5), the morphological evolution of ceramsite with different Fe_2O_3 additions was analyzed.

At lower temperatures, as illustrated in Fig. 6, the projected area remained relatively unchanged regardless of Fe_2O_3 concentration. This is due to limited mass transfer and a weak sintering driving force between CFB fly ash particles, indicating that solid-state sintering was predominant [44], [45]. However, as the temperature and holding time increased, the ceramsite entered liquid-phase sintering, leading to a significant reduction in its projected area. The shrinkage intensified with rising temperature, highlighting the dominant role of the liquid phase in shaping the final structure.

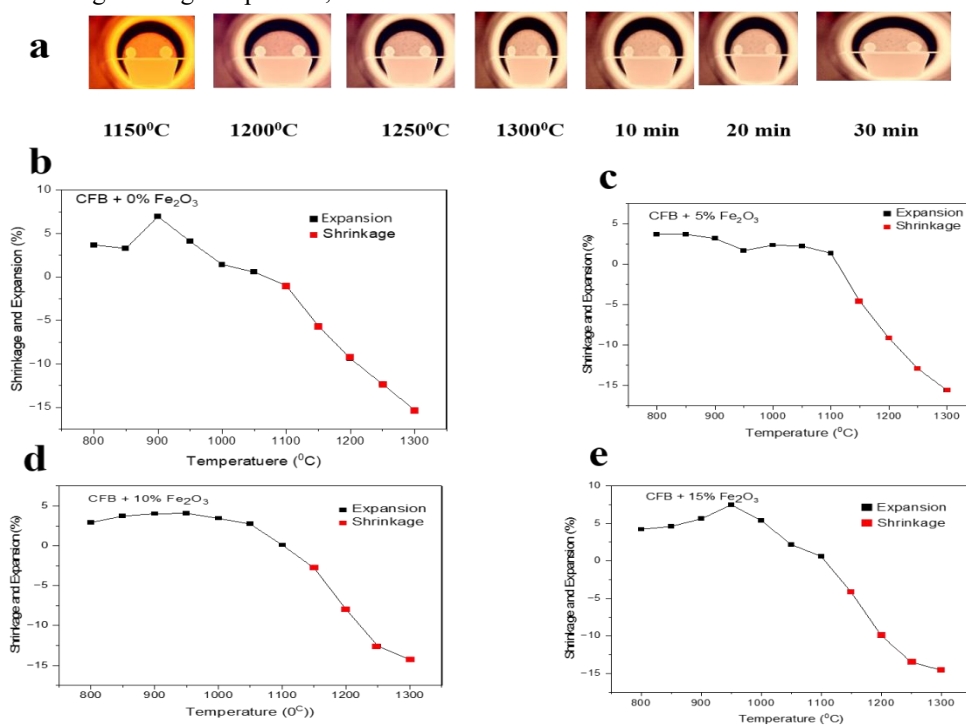


Fig. 6. Solid-liquid sintering of ceramsite at 1300°C with varying ratios of Fe_2O_3 addition

3.3 Effect of Fe_2O_3 on the Shrinkage and Expansion Behavior of Ceramsite during Sintering

The sintering process has a significant impact on ceramsite's final characteristics, particularly its expansion and shrinkage. The addition of Fe_2O_3 changes these characteristics and affects the material's structural stability and strength. The ceramsite sample containing 0 wt% Fe_2O_3 exhibited the most uncontrolled expansion at 900°C , reaching 6.95%. This behavior suggests significant gas retention in the material because there is no fluxing agent to

regulate the bloating process. At 1100°C , however, the sample started to shrink (-1.01%). The sintering driving force was insufficient at temperatures below 1100°C , and the breakdown of carbonates and other materials, along with the combustion of remaining carbon, only slightly expanded the material. This expansion dropped as the temperature increased. According to Table 1, the loss on ignition (LOI) of CFB fly ash was relatively low at 2.53%, primarily due to the burning of residual carbon. When the temperature remained below 1100°C , this combustion did not generate

enough heat to melt minerals such as mullite, corundum, and anorthite, resulting in minimal expansion of the ceramsite. As the temperature rose above 1100°C, liquid-phase sintering took over, leading to continuous shrinkage as the liquid-phase content increased. By 1250°C, the sample had shrunk by 12.34%, and at 1300°C, shrinkage reached 15.29%. These findings suggest that, without Fe₂O₃, ceramsite lacks the necessary structural control, causing excessive shrinkage during densification.

The expansion phase improved when 5 wt% Fe₂O₃ was added; at 850°C, the maximum expansion was 3.69%. Fe₂O₃ acts as a stabilizing agent, preventing excessive bloating, as observed in this sample compared with the 0 wt% Fe₂O₃ sample. The decrease started at 1150°C (-4.59%), and it increased at 1250°C (-12.92%). At 1300°C, the sample showed the greatest shrinkage of any composition at -15.58%. The results suggest that Fe₂O₃ addition had a significant impact on ceramsite sintering, accelerating the process and reducing the temperature range required for stable shrinkage. Within the optimal temperature range, the formation of an abundant liquid phase contributed to improved compressive strength. The shrinkage rate of the ceramsite's projected area was measured from the initial sintering temperature (T_{is}) to the end of the heating process. The results showed that when Fe₂O₃ was added at 0 wt%, 5 wt%, 10 wt%, and 15 wt%, the shrinkage rates were 15.29%, 15.58%, 14.29%, and 14.56%, respectively, indicating an initial increase followed by a decline. However, at Fe₂O₃

levels of 10 wt% and 15 wt%, shrinkage rates declined to 14.29% and 14.56%, respectively. This suggests that excessive Fe₂O₃ reduced the viscosity of the liquid phase, affecting the development of the pore structure [46], thereby limiting densification and weakening compressive strength. The slight increase in shrinkage from 15.29% (0 wt% Fe₂O₃) to 15.58% (5 wt% Fe₂O₃) can be attributed to the reaction of Fe₂O₃ with SiO₂ and Al₂O₃ in CFB fly ash at high temperatures. This reaction facilitated the formation of a low-melting liquid phase, which filled gaps between unmelted particles and promoted densification. The reduction in unmelted solid particles, combined with surface tension effects, helped improve the material's density and compressive strength while decreasing porosity [47].

3.4 Effect of crystalline phase on compressive strength

The influence of sintering temperature and Fe₂O₃ concentration on ceramsite formation was analyzed using X-ray diffraction (XRD) at varying temperatures and Fe₂O₃ levels. Specifically, the ceramsite's composition and mineral phase distribution were examined with 5 wt% Fe₂O₃. As presented Figure 7 and Table 2, the primary crystalline phases identified included mullite, cristobalite, anorthite, pyroxene, magnetite, hercynite, and a minor fraction of fayalite. The results indicate that ceramsite's mineral phase composition undergoes significant changes as the sintering temperature increases from 1150°C to 1300°C.

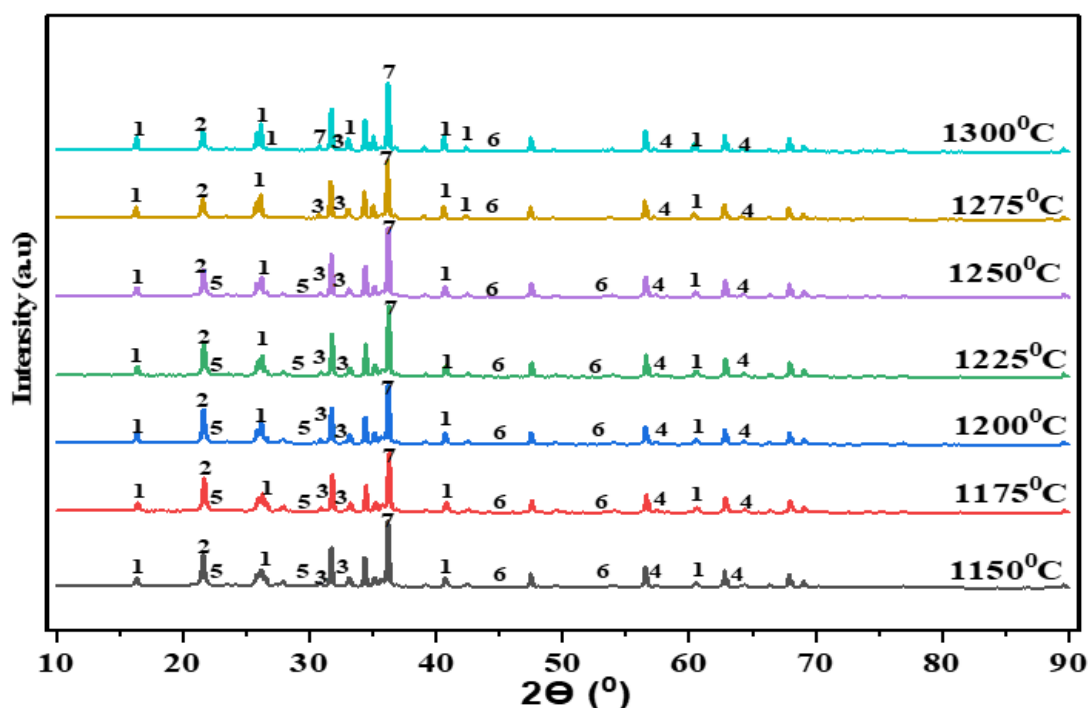


Fig. 7. XRD analyses of ceramsite with 5 wt% Fe₂O₃ at varying sintering temperatures

1-Mullite (3Al₂O₃·2SiO₂); 2- Cristobalite (SiO₂); 3-Pyroxene Ca(Mg,Fe)Si₂O₆, 4-Magnetite (Fe₃O₄); 5-Anorthite (CaAl₂Si₂O₈); 6 Fayalite (Fe₂SiO₄); 7-Hercynite (FeAl₂O₄)

XRD analysis revealed a progressive increase in the formation of mullite, hercynite, and pyroxene-type silicates with rising temperature. Mullite began forming at 1150°C and increased significantly between 1200°C and 1275°C, showing sustained intensity at 1300°C. It is the primary phase contributing to high compressive strength due to its interlocking, needle-like microstructure. Hercynite emerged at $\geq 1150^\circ\text{C}$ as a spinel product of Fe_2O_3 and Al_2O_3 interaction, playing a role in microstructural densification and thermal stability. Pyroxene phases appeared from 1200°C, contributing to compactness and moderate strength improvement. In contrast, fayalite, a weaker phase with lower hardness, appeared transiently at mid-temperatures but diminished at higher sintering temperatures, thereby reducing its negative impact on strength.

The addition of Fe_2O_3 strongly influenced the crystallization pathway by promoting spinel (hercynite) formation, reducing brittle cristobalite content, and encouraging the development of pyroxene and minor magnetite phases. These changes suppressed the formation of glassy or amorphous phases and improved the overall crystallinity of the ceramsite. As sintering temperature increased, the presence of cristobalite and fayalite diminished, while stable crystalline structures such as mullite and hercynite dominated, leading to a more thermally stable and mechanically robust matrix.

A strong correlation was observed between phase composition and compressive strength. At 1150°C, incomplete sintering and the presence of weak phases resulted in low strength. As the temperature rose to 1175°C and 1200°C, the formation of hercynite and pyroxene improved strength moderately. Optimal phase development occurred between 1275°C and 1300°C, where fayalite was nearly absent and mullite and hercynite peaked, resulting in the highest compressive strength. This confirms that 5 wt% Fe_2O_3 acts as a sintering aid and crystallization promoter, significantly enhancing the performance of CFB fly ash-based ceramsite.

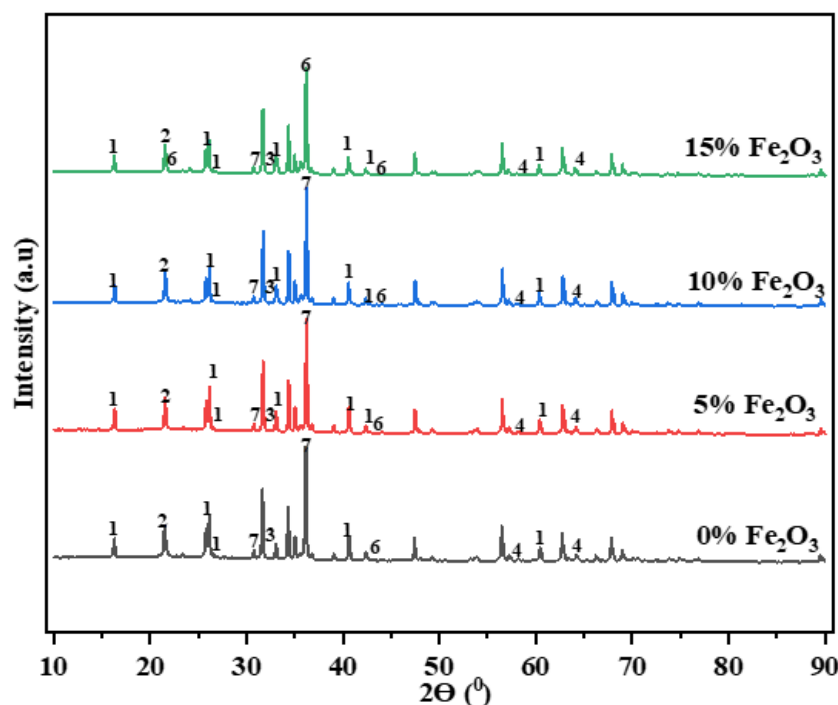


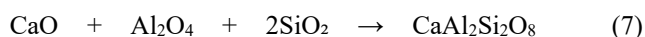
Fig. 8. XRD analysis of ceramsite produced at 1300°C with varying ratios of Fe_2O_3 addition

1-Mullite ($3\text{Al}_2\text{O}_3 \cdot 2\text{SiO}_2$); 2- Cristobalite (SiO_2); 3-Pyroxene $\text{Ca}(\text{Mg,Fe})\text{Si}_2\text{O}_6$, 4-Magnetite (Fe_3O_4); 5-Anorthite ($\text{CaAl}_2\text{Si}_2\text{O}_8$); 6 Fayalite (Fe_2SiO_4); 7-Hercynite (FeAl_2O_4)

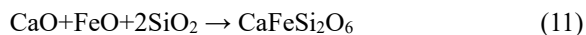
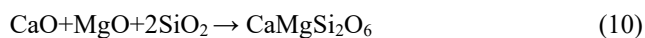
The XRD data, as illustrated in Eqs. (6), (7), (8), and (9), demonstrated that Fe_2O_3 played a crucial role in the formation of key mineral phases, including mullite, cristobalite, pyroxene, magnetite, fayalite, and hercynite, at different sintering temperatures. The mullite phase developed more rapidly as temperature increased (Eq. (6)), while the presence of Fe_2O_3 actively promoted the

formation of hercynite, a mineral that enhanced liquid-phase sintering. This process contributed to the development of a dense, hercynite-rich network, which reinforced the silicate matrix, lowered porosity, and improved the compactness of ceramsite, ultimately leading to higher compressive strength [48].

However, when Fe₂O₃ content was increased further, the fayalite peaks became more prominent. The excess Fe₂O₃ negatively affected the stability of the crystal structure, causing over-melting and an increase in brittleness [40], which weakened the material's compressive strength. These mineral phase transformations during ceramsite sintering are described by the reactions in Eqs. (6), (7), (8), (9), (10) and (11).



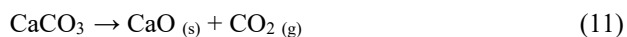
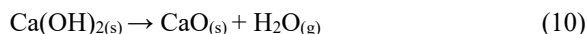
Formation of pyroxenes (diopside and hedenbergite)



3.6 TG-DSC-FTIR Analysis

To examine weight loss dynamics and heat transfer mechanisms during ceramsite sintering, a thermogravimetric-differential scanning calorimetry (TG-DSC) analysis was conducted on CFB fly ash with Fe₂O₃ additions of 5 wt%, 10 wt%, and 15 wt% in an air atmosphere. As depicted in Fig. 8, the weight loss behavior of the four raw material samples follows a pattern that can be divided into three distinct phases, corresponding to substance volatilization at varying temperatures. The CFB fly ash sample's thermal reactions are highlighted in Fig. 8a, showing a total weight loss of approximately 3.74%, as evidenced by the TG curve, with noticeable weight loss phases occurring at different temperature ranges.

The initial weight loss phase, lasting approximately 100 minutes, results from the evaporation of free water, the breakdown of crystalline water, and minor desorption. As per Eq. (10), further weight loss beyond 160 minutes can be attributed to the thermal decomposition of Ca(OH)₂ and CaCO₃ in CFB fly ash. Subsequently, at 190 minutes, the material undergoes carbon combustion and additional CaCO₃ decomposition, as illustrated in Eq. (11). These transformations align well with the thermal events recorded in the DSC curve.



The weight loss behavior shown in Figures 8(b)–(d) follows a trend similar to that of CFB fly ash. A first endothermic peak appears between 100°C and 200°C, attributed to dehydration, which becomes more pronounced with increasing Fe₂O₃ content. Between 250°C and 400°C, a second endothermic peak suggests processes like carbon

oxidation or the decomposition of carbonates. An important exothermic peak emerges between 600°C and 900°C, which is linked to the crystallization and development of silicate phases, such as calcium silicate and mullite, along with iron-containing phases like ferrite and hematite [26]. A smaller exothermic peak around 1000°C to 1200°C likely indicates the transition of iron-rich phases. For the sample with 5 wt.% Fe₂O₃, an additional exothermic peak above 1200°C was observed, marking the occurrence of high-temperature sintering.

Using TG-DSC-FTIR analysis, the thermochemical behaviour of CFB fly ash and the formation of gas phases during ceramsite sintering were investigated. Results from CFB fly ash samples with varying Fe₂O₃ additions (0–15%) show important findings into the evolution of CO₂ and thermochemical reactions. The infrared absorption peaks associated with CO₂ were predominantly detected in the wavelength range of 2300–2400 cm⁻¹. This is correlated with carbonate decomposition or organic oxidation, with the intensity and position varying significantly with the Fe₂O₃ content and temperature. Compared with undoped ash, higher Fe₂O₃ concentrations (5–15%) attenuate the peak intensity (Fig. 9a–d), suggesting that Fe₂O₃ suppresses CO₂ generation by stabilizing carbon phases or promoting redox reactions that limit carbonate breakdown. The temperature-dependent behavior further shows that CO₂ release occurs in stages: minor peaks below 600°C correspond to labile carbonates, whereas stronger peaks at higher temperatures arise from refractory carbonates or silicate-bound CO₃²⁻. The Fe₂O₃-doped samples exhibit delayed or broadened peaks, indicating the altered thermal stability of the carbonaceous components. This moderate gas release may increase the sintering kinetics by reducing pore formation, thereby increasing the ceramsite density.

The interaction between Fe₂O₃ and fly ash involves both physical and chemical mechanisms. Fe₂O₃ acts as a flux, lowering silicate melting points to promote liquid-phase sintering, which encapsulates carbonates and delays decomposition, minimizing abrupt CO₂ release. Additionally, Fe³⁺ facilitates redox reactions, oxidizing residual carbon or sulfur compounds into non-gaseous intermediates and indirectly suppressing CO₂. The optimal Fe₂O₃ content at a ratio of 5 wt% to 10 wt% balances gas management and sintering efficiency, yielding ceramsite with reduced porosity and enhanced mechanical strength. These findings highlight the dual role of Fe₂O₃ in modulating reaction pathways and microstructural development, offering a strategic approach to optimize industrial waste valorization processes while aligning with sustainability goals through controlled gas emissions.

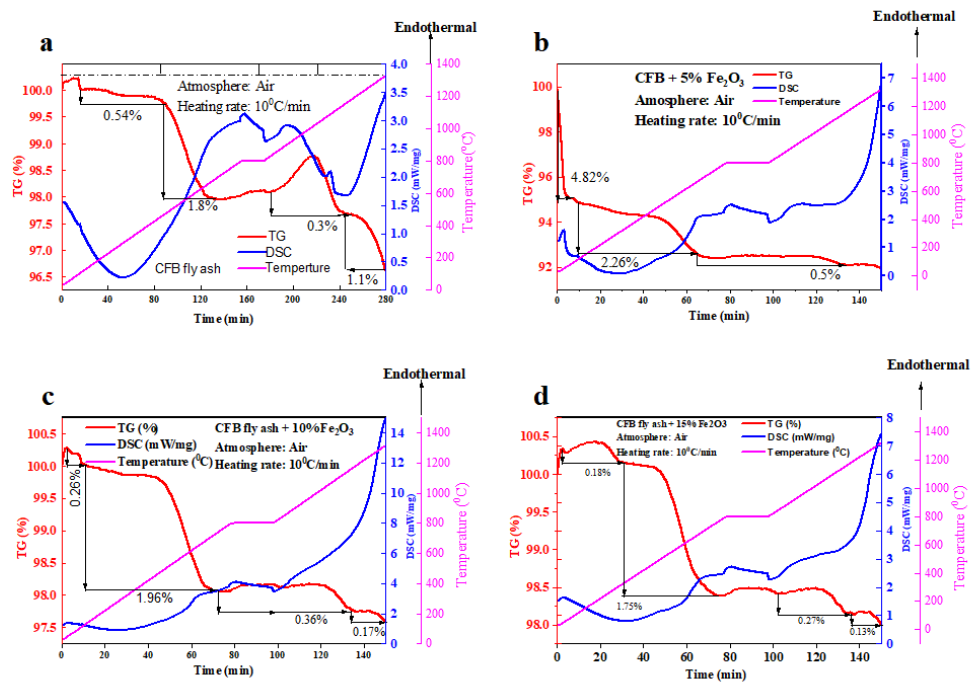


Fig. 9 Thermal analysis TG-DSC curves of CFB fly ash with different Fe_2O_3 addition

(a) CFB+0 wt% Fe_2O_3 ; (b) CFB+ 5 wt% Fe_2O_3 ; (c) CFB + 10 wt% Fe_2O_3 ; and (d) CFB+ 15 wt% Fe_2O_3

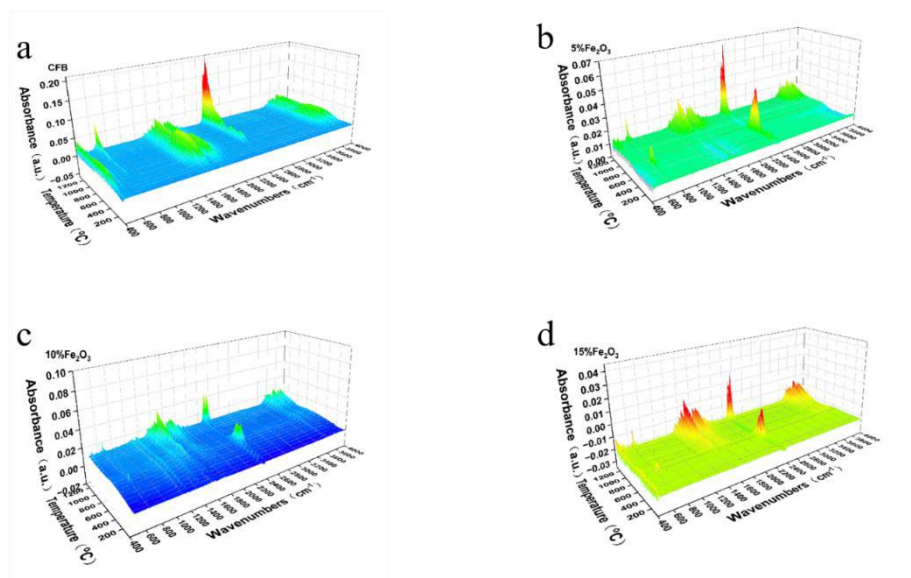


Fig. 10. FTIR analysis of CFB fly ash across a range of temperatures

(a) CFB + 0 wt% Fe_2O_3 ; (b) CFB + 5wt% Fe_2O_3 ; (c) CFB + 10wt% Fe_2O_3 and (d) CFB + 15wt% Fe_2O_3

3.7 Sintering mechanism of high-strength ceramsite

High-strength ceramsite made from circulating fluidized bed (CFB) fly ash is sintered through an intricate

process of thermal, chemical, and microstructural changes, with the addition of Fe_2O_3 having a particularly significant impact. Sintering begins as a thermally induced process that

causes densification, phase changes, and particle rearrangement [43], [46]. Three main phases make up the sintering process for ceramsite: initial neck development between particles, middle densification marked by pore contraction, and final grain growth, in which liquid-phase creation is important. Fe_2O_3 , which functions as a fluxing agent, greatly improves the sintering process. In order to create low-melting-point eutectics like hercynite (FeAl_2O_4), Fe_2O_3 reacts with alumina (Al_2O_3) to lower the sintering temperature. Through viscous flow and grain boundary diffusion, these phases encourage the formation of a temporary liquid phase, which improves mass transport and makes particle rearrangement easier. As a result, there is less porosity, better particle bonding, and greater structural integrity [49].

In particular, the liquid-phase sintering process is optimized at moderate Fe_2O_3 concentrations (5 – 10 wt%). The liquid phase creates a dense microstructure with smaller pores, fills in interstitial spaces, and promotes the growth of crystalline phases, particularly mullite. A compact matrix and enhanced interparticle adhesion are revealed by SEM examination at this composition. Furthermore, Fe_2O_3 stabilizes carbon phases, moderates gas release, and delay thermal breakdown, all of which stop pore coarsening and bubble formation, according to FTIR and TG-DSC-FTIR investigations. However, excessive Fe_2O_3 additions (>10 wt%) result in over-fluxing, leading to excessive liquid-phase formation. This disrupts the balance between densification and bloating, increasing porosity due to uncontrolled gas release and the formation of large pores and microcracks. These structural defects reduce compressive strength and compromise the integrity of the ceramsite. According to morphological investigations, sintering at lower temperatures (1150–1175°C) produces poor densification and insufficient liquid-phase development. On the other hand, maximum shrinkage, improved densification, and minimal porosity are obtained by sintering at 1300°C with an ideal Fe_2O_3 concentration, suggesting a dominant liquid-phase sintering mechanism.

In conclusion, temperature-dependent phase transitions and the fluxing behaviour of Fe_2O_3 control the sintering mechanism of high-strength ceramsite. Through regulated liquid-phase sintering, a dense microstructure and stable crystalline phases are encouraged by an optimum Fe_2O_3 concentration. Achieving higher structural qualities and promoting the sustainable use of CFB fly ash in high-performance building materials depend on this mechanism.

3.8 Microscopic morphology analysis on compressive strength

Figure 11 shows the SEM analysis of ceramsite sintered at 1150°C and 1300°C, with Fe_2O_3 concentrations of 0 wt% and 5 wt%. The microstructure reveals how both sintering temperature and Fe_2O_3 influence the ceramsite's shape and density. The CFB fly ash sample fired at 1150°C (Figure 11a) has a rough, porous surface with little densification, which suggests that sintering was incomplete. When 5 wt.% Fe_2O_3 is added (Figure 11b), the pores become closed and better connected, showing some improvement in densification. This suggests that Fe_2O_3 may be acting as a flux, helping the sintering process begin. However, the overall porosity is still high, indicating that 1150°C is not enough to fully vitrify the material and improve its strength. The irregular pores and limited liquid-phase formation prevented the ceramsite from achieving the necessary compressive strength, as required by the Chinese National Standard. Thus, lower sintering temperatures do not result in the creation of high-strength ceramsite.

When the sintering temperature was increased to 1300°C, there was a clear improvement in the densification of the ceramsite. The CFB fly ash sample without Fe_2O_3 (Figure 11c) showed much less porosity, though a small crack remained, likely due to shrinkage or too much heat. The central cross-section of the ceramsite appeared smoother, with fine fractures between 10 and 40 μm and small connected pores of 5 to 10 μm in size. The higher temperature caused the CFB fly ash particles to melt, forming a liquid phase that flattened some of the sintered surfaces. However, the liquid phase at this stage was not enough to fill all the internal pores of the ceramsite. As a result, after cooling, the ceramsite had many communication pores, due to the interaction between gas and liquid phases.

At 1300°C, the 5 wt.% Fe_2O_3 -modified sample showed excellent sintering behavior, with better densification and much lower porosity, as seen in Figure 11d. The liquid phase formed by the reaction of Fe_2O_3 at high temperatures played an important role in improving the ceramsite's densification and reducing its porosity, which ultimately enhanced its compressive strength. This liquid phase development also helped to minimize the small amount of gas produced during sintering, further boosting the ceramsite's strength [27].

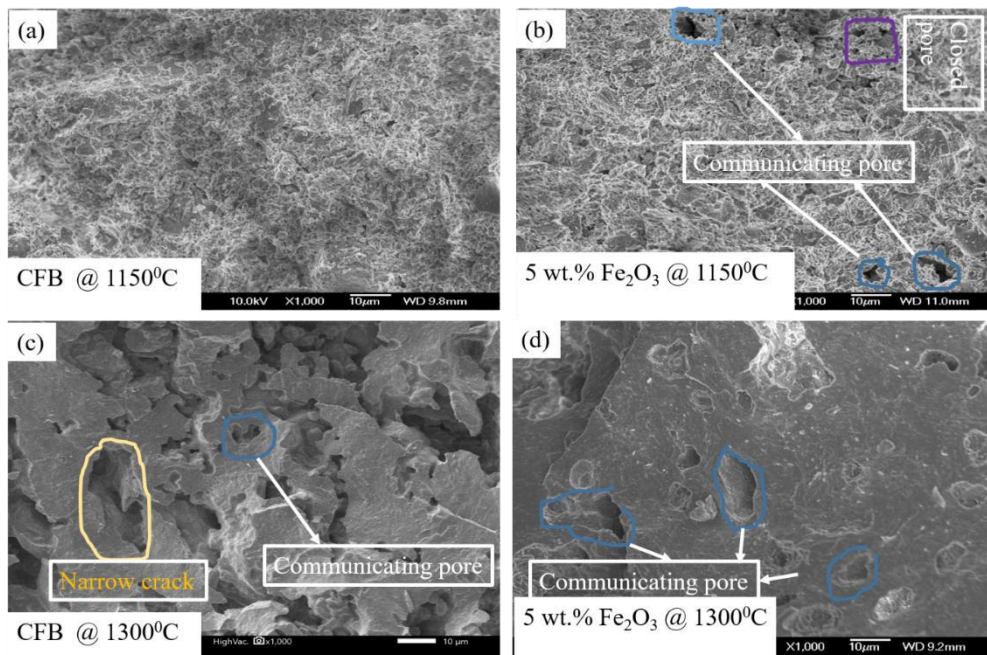


Fig. 11. Scanning electron microscopy (SEM) images showing the effect of Fe_2O_3 additive on the ceramsite at different sintering temperatures with 0 - 5wt% Fe_2O_3 addition

(a) CFB @ 1150°C; (b) 5wt.% Fe_2O_3 @ 1150°C; (c) CFB @ 1300°C; (d) 5wt.% Fe_2O_3 @ 1300°C

At 1200°C with 5 wt.% Fe_2O_3 (Fig. 12a), the microstructure is highly porous with disordered particle distribution, revealing poor sintering and weak interparticle bonding. The prevalence of micro-cracks and pores certifies that the material has not reached densification, and this could be detrimental to its mechanical strength and durability. This partial sintering is because of insufficient thermal energy to produce efficient diffusion and bonding among the particles. The material shows less porosity and better particle bonding as the temperature rises to 1250°C (Fig. 12b). The smoother surfaces indicate that liquid-phase sintering has begun, which improves densification. Even still, there are still some residual voids, suggesting that although the material is getting denser, full densification has not yet been reached.

The microstructure becomes noticeably denser at 1300°C with 5 wt% Fe_2O_3 (Fig. 12c), showing a clear sign of material aggregation and fewer visible pores. This implies that the sintering process has advanced to a point

where improved particle rearrangement and densification are possible due to adequate liquid-phase formation. At this point, a glassy phase may emerge, which could increase the material's mechanical strength and resistance to external forces.

However, the microstructure displays bigger interconnected pores when the Fe_2O_3 content is raised to 10 wt% at the same temperature (Fig. 12d). This might be because of too much liquid-phase formation, which causes gas release or bloating during sintering. Grain boundary cracks provide additional evidence that the material's structural integrity may have been compromised by high temperatures. However, higher temperatures generally improve sintering and decrease porosity up to a certain degree, but too much Fe_2O_3 at high temperatures might have negative impacts like bloating. 5 wt% Fe_2O_3 at 1300°C is the optimum ratio for producing a high-strength ceramsite, where sintering is well-developed without having too much porosity.

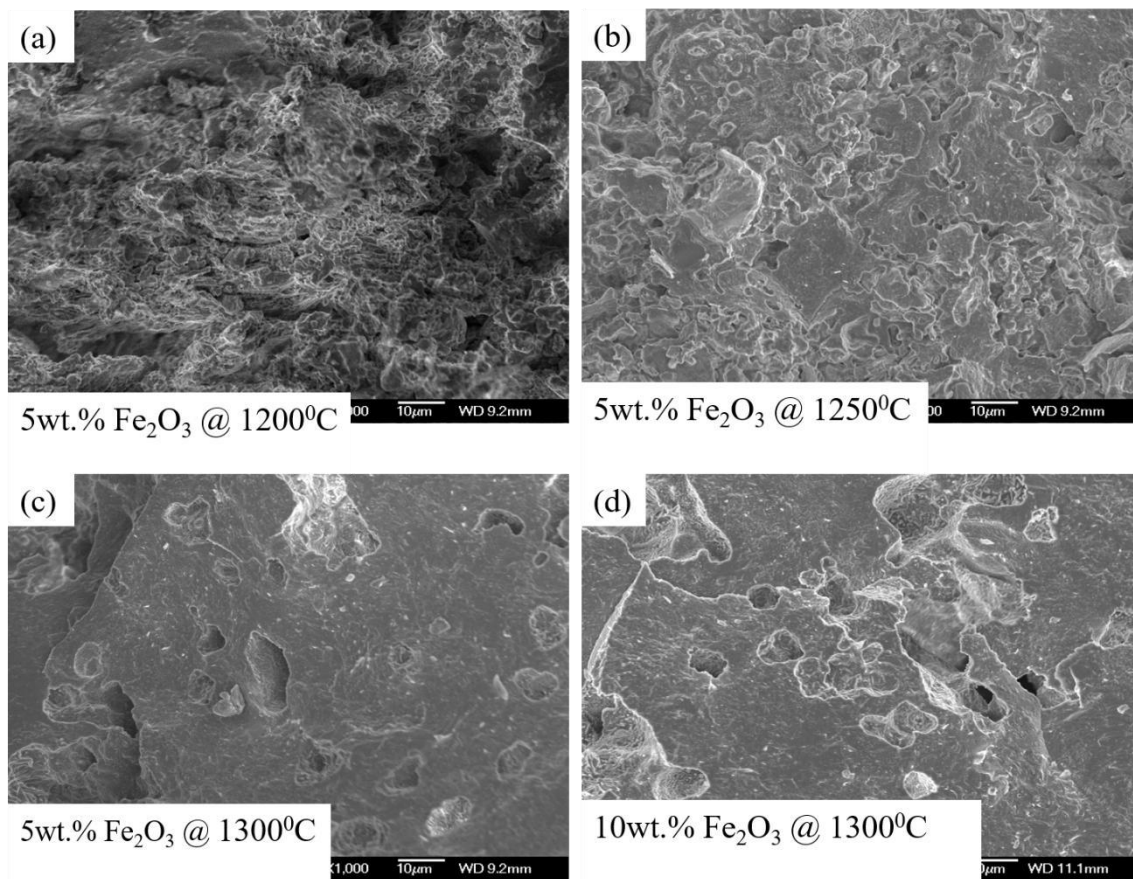


Fig. 12. Scanning electron microscopy (SEM) of ceramsite at varying sintering temperatures with 5 wt% - 10 wt% Fe_2O_3 addition

(a) 5wt.% Fe_2O_3 @ 1200°C; (b) 5wt.% Fe_2O_3 @ 1250°C; (c) 5wt.% Fe_2O_3 @ 1300°C; (d) 10wt.% Fe_2O_3 @ 1300°C

IV. CONCLUSION

This study revealed that adding Fe_2O_3 in a controlled manner greatly improves both the sintering properties and the mechanical performance of ceramsite made from CFB fly ash. Under the best conditions, which involved adding 5 wt% Fe_2O_3 and sintering at 1300°C, the ceramsite achieved a compressive strength of 36.09 MPa, which is significantly higher than the 16.38 MPa observed in samples without Fe_2O_3 . Water absorption also dropped dramatically, from 12.20% at 1225°C to only 0.19% at 1300°C, while both the apparent and stacking densities increased, rising from 1770.23 kg/m³ to 2327.85 kg/m³ and from 863.94 kg/m³ to 1189.3 kg/m³, respectively. The XRD and SEM analyses showed that Fe_2O_3 promoted the formation of a mullite-rich matrix and improved liquid-phase sintering, which enhanced particle bonding and created a more uniform pore structure. The shrinkage at 1300°C with 5 wt% Fe_2O_3 was around -15.58%, contributing to superior densification. However, when the Fe_2O_3 content was increased beyond 5 wt%, overfluxing occurred, which reduced the liquid phase

viscosity, leading to a slight decrease in compressive strength and densification. Overall, these findings confirm that the controlled addition of Fe_2O_3 improves ceramsite's microstructure and performance, offering a sustainable approach for turning industrial waste into high-strength construction materials.

DECLARATION OF AUTHORSHIP AND CONTRIBUTIONS

Ikechukwu Okeke and Peng Liyang contributed equally to the experimental design, data interpretation, and manuscript writing. Chibuikie Chiemelie and Paul Afreh assisted in material preparation and lab analysis. Mahwish Islam contributed to data validation and editing. Prof. Qin Yuhong supervised the project and approved the final manuscript.

DECLARATION OF COMPETING INTEREST

The authors state that they have no competing financial interests or personal relationships that may have influenced the findings in this paper.

REFERENCES

- [1] W. Zhang, S. Wang, J. Ran, H. Lin, W. Kang, and J. Zhu, "Research progress on the performance of circulating fluidized bed combustion ash and its utilization in China," *Journal of Building Engineering*, vol. 52, p. 104350, 2022.
- [2] X. Chen, J. Gao, Y. Yan, and Y. Liu, "Investigation of expansion properties of cement paste with circulating fluidized bed fly ash," *Construction and Building Materials*, vol. 157, pp. 1154–1162, Dec. 2017, doi: 10.1016/j.conbuildmat.2017.08.159.
- [3] R. Siddique, "Use of municipal solid waste ash in concrete," *Resources, Conservation and Recycling*, vol. 55, no. 2, pp. 83–91, 2010.
- [4] X. Shan, Z. Ma, Y. Guo, and F. Cheng, "Study on characteristics of circulating fluidized bed pulverized fuel ash with different particle sizes," *Coal Science and Technology*, vol. 46, no. 11, pp. 232–238, 2018.
- [5] M. Ning, Z. Wang, J. Qian, and S. Tang, "Characteristics of fluidized bed coal combustion fly ash and slag and its adaptability with current standards," *Bulletin of the Chinese Ceramic Society*, vol. 38, no. 3, pp. 688–693, 2019.
- [6] K. He, Z. Lu, J. Li, and K. Song, "Comparative study on properties of circulating fluidized bed combustion ash and slag," *Journal of Wuhan University of Technology*, vol. 36, no. 3, pp. 6–13, 2014.
- [7] J.-S. QIAN, Z.-W. ZHANG, H.-W. ZHENG, and Z. WANG, "Study on the varieties and distribution of sulfur minerals in CFBC ash/slag," *Journal of China Coal Society*, vol. 38, no. 4, pp. 651–656, 2013.
- [8] A. González, N. Moreno, R. Navia, and X. Querol, "Study of a Chilean petroleum coke fluidized bed combustion fly ash and its potential application in copper, lead and hexavalent chromium removal," *Fuel*, vol. 89, no. 10, pp. 3012–3021, 2010.
- [9] D. Qiao, J. Qian, Q. Wang, Y. Dang, H. Zhang, and D. Zeng, "Utilization of sulfate-rich solid wastes in rural road construction in the Three Gorges Reservoir," *Resources, conservation and recycling*, vol. 54, no. 12, pp. 1368–1376, 2010.
- [10] H.-A. Nguyen, T.-P. Chang, J.-Y. Shih, C.-T. Chen, and T.-D. Nguyen, "Influence of circulating fluidized bed combustion (CFBC) fly ash on properties of modified high volume low calcium fly ash (HVFA) cement paste," *Construction and Building Materials*, vol. 91, pp. 208–215, Aug. 2015, doi: 10.1016/j.conbuildmat.2015.05.075.
- [11] T. Ji, D.-D. Zheng, X.-F. Chen, X.-J. Lin, and H.-C. Wu, "Effect of prewetting degree of ceramsite on the early-age autogenous shrinkage of lightweight aggregate concrete," *Construction and Building Materials*, vol. 98, pp. 102–111, Nov. 2015, doi: 10.1016/j.conbuildmat.2015.08.102.
- [12] J. Qin, C. Cui, X. Cui, A. Hussain, and C. Yang, "Preparation and characterization of ceramsite from lime mud and coal fly ash," *Construction and Building Materials*, vol. 95, pp. 10–17, Oct. 2015, doi: 10.1016/j.conbuildmat.2015.07.106.
- [13] J. Pei, X. Pan, Y. Qi, H. Yu, and G. Tu, "Preparation and characterization of ultra-lightweight ceramsite using non-expanded clay and waste sawdust," *Construction and Building Materials*, vol. 346, p. 128410, Sep. 2022, doi: 10.1016/j.conbuildmat.2022.128410.
- [14] T. Yu, Z. Zhao, and J. Li, "Effect of sintering temperature and sintering additives on the properties of alumina ceramics fabricated by binder jetting," *Ceramics International*, vol. 49, no. 6, pp. 9948–9955, 2023.
- [15] Y. Long et al., "Preparation of High-strength ceramsite from municipal solid waste incineration fly ash and clay based on CaO-SiO₂-Al₂O₃ system," *Construction and Building Materials*, vol. 368, p. 130492, Mar. 2023, doi: 10.1016/j.conbuildmat.2023.130492.
- [16] T. Li, T. Sun, and D. Li, "Preparation, sintering behavior, and expansion performance of ceramsite filter media from dewatered sewage sludge, coal fly ash, and river sediment," *Journal of material cycles and waste management*, vol. 20, pp. 71–79, 2018.
- [17] S. Hua, D. Wu, J. Wu, S. Li, G. Liu, and D. Pei, "Characterization of the physical chemistry properties of iron-tailing-based ceramsite," *Molecules*, vol. 28, no. 5, p. 2258, 2023.
- [18] X. Wang, Y. Jin, Z. Wang, Y. Nie, Q. Huang, and Q. Wang, "Development of lightweight aggregate from dry sewage sludge and coal ash," *Waste management*, vol. 29, no. 4, pp. 1330–1335, 2009.
- [19] Z. Yang, W. Song, J. Yang, L. Deng, Z. Cao, and M. Shi, "High-strength ceramsite made with sludge and low-quality fly ash," *Journal of materials in civil engineering*, vol. 25, no. 7, pp. 851–856, 2013.
- [20] C. Ou et al., "Removal of ammonia nitrogen and phosphorus by porous slow-release Ca²⁺ ceramsite prepared from industrial solid wastes," *Separation and Purification Technology*, vol. 304, p. 122366, Jan. 2023, doi: 10.1016/j.seppur.2022.122366.
- [21] M. Liu, Z. Zhu, Z. Zhang, Y. Chu, B. Yuan, and Z. Wei, "Development of highly porous mullite whisker ceramic membranes for oil-in-water separation and resource utilization of coal gangue," *Separation and Purification Technology*, vol. 237, p. 116483, Apr. 2020, doi: 10.1016/j.seppur.2019.116483.
- [22] General Administration of Quality Supervision, "Inspection and Quarantine of the People's Republic of China, China National Standardization Administration Committee, Lightweight Aggregates and its Test Methods—Part 1: Lightweight Aggregates," Standards Press of China, Beijing, 2010.
- [23] China Association for Engineering Construction Standardization, "High Strength Lightweight Aggregate," Standards Press of China, Beijing, 2020.
- [24] C. M. Riley, "Relation of chemical properties to the bloating of clays," *Journal of the American ceramic society*, vol. 34, no. 4, pp. 121–128, 1951.

- [25] D. Lindberg, C. Molin, and M. Hupa, "Thermal treatment of solid residues from WtE units: A review," *Waste Management*, vol. 37, pp. 82–94, Mar. 2015, doi: 10.1016/j.wasman.2014.12.009.
- [26] X. Wu et al., "Preparing high-strength ceramsite from ferronickel slag and municipal solid waste incineration fly ash," *Ceramics International*, vol. 48, no. 23, Part A, pp. 34265–34272, Dec. 2022, doi: 10.1016/j.ceramint.2022.07.357.
- [27] M. Liu, C. Wang, Y. Bai, and G. Xu, "Effects of sintering temperature on the characteristics of lightweight aggregate made from sewage sludge and river sediment," *Journal of Alloys and Compounds*, vol. 748, pp. 522–527, Jun. 2018, doi: 10.1016/j.jallcom.2018.03.216.
- [28] B. Ma, Y. Li, G. Liu, and D. Liang, "Preparation and properties of Al₂O₃–MgAl₂O₄ ceramic foams," *Ceramics International*, vol. 41, no. 2, pp. 3237–3244, 2015.
- [29] L. Wang et al., "Red mud-enhanced magnesium phosphate cement for remediation of Pb and As contaminated soil," *Journal of Hazardous Materials*, vol. 400, p. 123317, Dec. 2020, doi: 10.1016/j.jhazmat.2020.123317.
- [30] Y. M. Wie, K. G. Lee, and K. H. Lee, "Chemical design of lightweight aggregate to prevent adhesion at bloating activation temperature," *Taylor & Francis*, Apr. 2020, Accessed: Jun. 24, 2024. [Online]. Available: <https://www.tandfonline.com/doi/abs/10.1080/21870764.2020.1725259>
- [31] J. Pei, X. Pan, Y. Qi, H. Yu, and G. Tu, "Preparation of ultra-lightweight ceramsite from red mud and immobilization of hazardous elements," *Journal of Environmental Chemical Engineering*, vol. 10, no. 4, p. 108157, Aug. 2022, doi: 10.1016/j.jece.2022.108157.
- [32] H. Mi, L. Yi, Q. Wu, J. Xia, and B. Zhang, "Preparation of high-strength ceramsite from red mud, fly ash, and bentonite," *Ceramics International*, vol. 47, no. 13, pp. 18218–18229, Jul. 2021, doi: 10.1016/j.ceramint.2021.03.141.
- [33] J. Zou, G. Xu, and G. Li, "Ceramsite obtained from water and wastewater sludge and its characteristics affected by Fe₂O₃, CaO, and MgO," *Journal of Hazardous Materials*, vol. 165, no. 1–3, pp. 995–1001, 2009.
- [34] S. China, "Lightweight Aggregates and its Test methods—Part 2: Test Methods for Lightweight Aggregates," *China Architecture & Building Press: Beijing, China*, 2010.
- [35] S. Yashima, Y. Kanda, and S. Sano, "Relationships between particle size and fracture energy or impact velocity required to fracture as estimated from single particle crushing," *Powder Technology*, vol. 51, no. 3, pp. 277–282, Aug. 1987, doi: 10.1016/0032-5910(87)80030-X.
- [36] Y. Li et al., "Measurement and statistics of single pellet mechanical strength of differently shaped catalysts," *Powder Technology*, vol. 113, no. 1, pp. 176–184, Nov. 2000, doi: 10.1016/S0032-5910(00)00231-X.
- [37] H. Wu et al., "Sintering-free preparation of porous ceramsite using low-temperature decomposing pore former and its sound-absorbing performance," *Construction and Building Materials*, vol. 171, pp. 367–376, May 2018, doi: 10.1016/j.conbuildmat.2018.03.152.
- [38] Y. Chen et al., "Adsorption mechanism of lead ions on porous ceramsite prepared by co-combustion ash of sewage sludge and biomass," *Science of The Total Environment*, vol. 702, p. 135017, Feb. 2020, doi: 10.1016/j.scitotenv.2019.135017.
- [39] J. Wang et al., "The role of residual char on ash flow behavior, Part 2: Effect of SiO₂/Al₂O₃ on ash fusibility and carbothermal reaction," *Fuel*, vol. 255, p. 115846, Nov. 2019, doi: 10.1016/j.fuel.2019.115846.
- [40] G. R. Xu, J. L. Zou, and G. B. Li, "Ceramsite obtained from water and wastewater sludge and its characteristics affected by (Fe₂O₃ + CaO + MgO)/(SiO₂ + Al₂O₃)," *Water Research*, vol. 43, no. 11, pp. 2885–2893, Jun. 2009, doi: 10.1016/j.watres.2009.03.046.
- [41] "Scopus preview - Scopus - Document details - Mixing water treatment residual with excavation waste soil in brick and artificial aggregate making." Accessed: Jan. 27, 2025. [Online]. Available: <https://www.scopus.com/record/display.uri?eid=2-s2.0-13244291562&origin=inward&txGid=40582fb43045979fab b17471f6f37f9d>
- [42] X. Zhenhua, L. Jianguo, S. Mingyong, and Z. Zhifei, "Effect of temperature on sintering ceramsite with sewage sludge and sediment," *Chinese Journal of Environmental Engineering*, vol. 7, no. 5, pp. 1894–1900, 2013.
- [43] C. Vakifahmetoglu and L. Karacasulu, "Cold sintering of ceramics and glasses: A review," *Current Opinion in Solid State and Materials Science*, vol. 24, no. 1, p. 100807, Feb. 2020, doi: 10.1016/j.cossms.2020.100807.
- [44] X. Wang et al., "Revealing the intrinsic sintering mechanism of high-strength ceramsite from CFB fly ash: Focus on the role of CaO," *Ceramics International*, Apr. 2024, doi: 10.1016/j.ceramint.2024.04.158.
- [45] Y. Qin et al., "Effect of biomass ash addition on coal ash fusion process under CO₂ atmosphere," *Fuel*, vol. 231, pp. 417–426, 2018.
- [46] R. M. German, P. Suri, and S. J. Park, "Liquid phase sintering," *Journal of materials science*, vol. 44, pp. 1–39, 2009.
- [47] H. Wang, J. Xu, Y. Liu, and L. Sheng, "Preparation of ceramsite from municipal sludge and its application in water treatment: A review," *Journal of Environmental Management*, vol. 287, p. 112374, Jun. 2021, doi: 10.1016/j.jenvman.2021.112374.
- [48] L. Zhang et al., "Investigation on coal ash fusibility and fluidity during the co-gasification of coal and coal indirect liquefaction residue," *Fuel Processing Technology*, vol. 221, p. 106949, Oct. 2021, doi: 10.1016/j.fuproc.2021.106949.
- [49] S.-M. Lee and S.-J. L. Kang, "Theoretical analysis of liquid-phase sintering: pore filling theory," *Acta Materialia*, vol. 46, no. 9, pp. 3191–3202, 1998.